New Nanocomposite Materials on the Basis of Dielectric Porous Matrices

Alexey Filimonov[1], Andrey Rudskoy[2], Aleksandr Naberezhnov[3], Sergey Vakhrushev[4], Ekaterina Koroleva[5], Igor Golosovsky[6], Yury Kumzerov[7]

[1-5,7]*St. Petersburg State Polytechnical University,* [3-5,7] *Ioffe Physical-Technical Institute,*

[6] *St. Petersburg Nuclear Physics Institute*

Abstract. **The correlations between physical properties and structure for various types of nanocomposite magnetic and ferroelectric materials on the basis of natural and artificial porous matrices have been studied by different experimental methods. The temperature evolution of structure, order parameter and dielectric response has been studied as a function of characteristic size of nanoparticles. The research has shown the existence of crossover of phase transition (PT) from the first order to the second one for ultra-small ferroelectric and magnetic particles.**

Keywords**: nanocomposites, porous matrices, neutron diffraction, dielectric response**

I. Introduction

The physical properties of nanostructured materials are one of the "hot" points of modern solid state physics and are not only of fundamental interest but also of practical importance. Indeed, it is shown that finite-size effects result in drastic changes of physical properties of ultra-dispersed materials. The observed phenomena become especially significant if the characteristic size of the dispersed particles becomes comparable with the correlation length of the order parameter critical fluctuations and the development of new nanotechnologies stimulates strongly the studies of various nanostructured and ultra-dispersed substances.

The experimental implementation of new effects in the physics of nanostructures relies upon our ability to create new types of structures and devices. Our understanding of material processing in the pursuit of ultra-small structures is steadily advancing. Epitaxial growth and lateral microstructuring techniques have made it possible to create low-dimensional electronic systems with quantum-confined structures, i.e., quantum wells, quantum wires, and quantum dots.

There are many methods for the preparation of such dispersed substances, and one of them is the intrusion of materials into artificial or natural porous matrices.

The embedding of substances into various porous matrices has some advantages over other methods:

- This method gives a possibility to produce nanostructures with a large range of controlled characteristic sizes from ~ 1 nm to ~300 nm.
- It is possible to prepare nanostructures with various geometry and topology: three-dimensional (3D) dendrite and regular structures, 2D film-like structures, 1D nanowires or 0D small nanoparticles.
- One can produce nanoparticles of various substances and compounds: metals, ferroelectrics, dielectrics, insulators, semiconductors, superconductors, magnetic materials and so on.
- It is possible to prepare a very large amount (up to several cubic centimeters) of nanocomposite materials (NCMs) (or materials in a restricted geometry). This enables us to use some experimental methods that require a large amount of nanostructures (for example neutron scattering, heat capacity measurements etc.).

Such NCMs have been extensively studied in recent years, and it has been shown that the reduction of physical size from the microscopic scale down to the meso- and nanoscopic scales results in a change of the majority of physical properties of NCMs, such as temperature and type of phase transitions (PT) [1–6], dielectric permittivity [7-9], atomic mobility of constituent ions [10-12], flowing of liquids in a confined geometry [12,13] and so on. One of the important aspects of NCMs is phase stability as a function of spatial dimension, geometry, topology and size of nanoparticles. The properties of NCMs and, in particular, of various types of PT (superconducting [14-16], superfluid [17,18], melting-freezing [6, 19-24], and other PTs [4, 7, 25-33] in different NCMs) have been extensively studied by calorimetry [19,21, 32], NMR [23,33-34], ultrasonic [35] and dielectric [7-9, 25] measurements, Raman [36,37], x-ray [26,28,30,38] and neutron scattering [4,6,11,39, 40-48], differential thermal analysis [49], etc. It has been shown that NCMs can form either a system of isolated particles [6] or a net of interconnected dendrite clusters [44,45], and their physical properties differ drastically from those in the corresponding bulk samples and strongly depend on different characteristics of porous matrices and embedded substances, such as pore size and geometry, wetting ability, surface tension, interaction between NCM and the surface of the host matrix, and so on.

This paper presents a review of properties and structure peculiarities of magnetic and ferroelectric nanocomposite materials on the basis of various artificial and natural porous matrices, such as porous glasses (3D dendrite interconnected net of nanochannels), artificial opals (3D regular net of nanocaverns), chrysotile asbestos (quasi-1D nanowires), MCM-41 and SBA-15.

II. Nanocomposites with Magnetic Ordering

The magnetic nanoparticles are of great interest because of their unique physical properties for practical applications. It has been shown that these properties drastically change in the

conditions of "restricted or confined geometry". These conditions assume:

- the number of atoms at the surface of nanoparticles becomes comparable with the total number of atoms;
- particle size is comparable with the length of the magnetic and atomic interaction.

Although the integral methods (e.g., Mössbauer spectroscopy, SQUID-measurements and others) have the higher luminosity and sensibility in contrast with diffraction, the physical interpretation of any experiment is impossible without knowledge of detailed magnetic and atomic structure of nanoparticles. Obviously, similar information can be obtained by the diffraction methods only, because the electronic (or other) microscopy does not provide the proper accuracy and resolution.

As host matrices, we used porous glasses with average pore diameter 70±3 Å, SBA-15 matrices with channels diameters of 47–87 Å and MCM-41 matrices with channels diameters of 24–35 Å. MnO, CoO and Fe_2O_3 were synthesized by a chemical bath deposition method. Manganese oxide was selected since the magnetic behaviour of the bulk was well studied. This oxide has an antiferromagnetic structure, for which the magnetic and nuclear Bragg reflections are well separated [50,51]. The magnetic order in bulk MnO occurs by a first order transition at 117±1 K [52], accompanied by a distortion of the cubic structure [51,53].

A. The magnetic Order inside and on the Surface of Nanoparticles

Reduction of magnetic moment. The first neutron diffraction experiments with nanoparticles in the condition of a "restricted geometry" were performed with the classic antiferromagnet MnO embedded into a porous glass [4]. Manganese oxide is very suitable for the studies of magnetism in the "restricted geometry". First, the oxide has a simple antiferromagnetic structure, for which the magnetic and nuclear Bragg reflections are well separated. Secondly, MnO is easily synthesized inside the cavities. Thus, it is possible to introduce a large quantity of oxide sufficient to perform neutron research. And third, manganese has a negative nuclear scattering length, while the oxygen has a positive scattering length. This provides a good contrast in the neutron diffraction that allows the controlling of stoichiometry with a high accuracy. At last, ion Mn^{2+} has a large magnetic moment of 5 μ_B/ion. The magnetic order in the bulk MnO occurs by a first order transition at ~ 117 K, accompanied by a distortion of the cubic structure [53]. Indeed, new Bragg reflections appearing below 122 K – Néel temperature – show the onset of the correlated magnetic order in the embedded nanoparticles (Fig. 1).

The diffraction lines are broadened with respect to the instrumental resolution, indicating that the correlation length is finite. The observed diffuse background is due to the porous silica glass. The indexing of the observed magnetic reflections corresponds to antiferromagnetic ordering similar to that for the bulk MnO. The shape of the reflections below the Néel temperature indicates structural distortions and matches to the trigonal distortion of a cubic lattice.

From the intensity of the magnetic Bragg reflections, the ordered magnetic moment at 10 K was found to be 3.84(4) μ_B/ion. This value, averaged over the magnetic region, turns out to be noticeably smaller than the experimental value of 4.892 μ_B/ion reported for MnO.

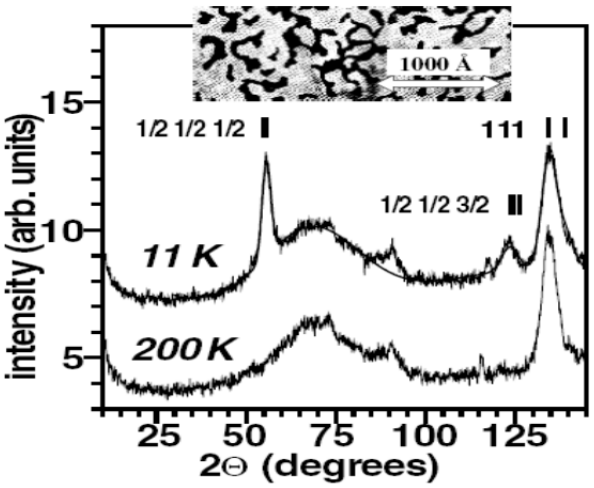

Fig. 1. Neutron diffraction patterns of MnO embedded into a porous glass. The stripes mark the positions of Bragg reflections corresponding to the trigonal distorted lattice. The solid line corresponds to the calculated profile. In the inset, the fragment of a typical micrograph of pore network in porous glasses is shown.

Moreover, the average size of a magnetic cluster turns out to be significantly smaller than the average size of a nanoparticle (Fig. 2). In the diffraction experiment, the surface spins, disordered on the atomic scale, do not contribute to the coherent magnetic Bragg reflections. Therefore, the reduction of the net moment can be easily explained by random moment canting. The difference between D_{mag} and D_{nucl} could be due to several factors. It could result from the breakdown of the large magnetic aggregates into smaller ones because of necks or other irregularities in the porous media. Another explanation could come from the random canting of spins at the surface of the nanoparticle near the pore walls and the formation of a "layer" with spin disorder. As a result, the orientation of the surface magnetic moments could be altered from that in the core. Such disordering is a well-established phenomenon for nanoparticles.

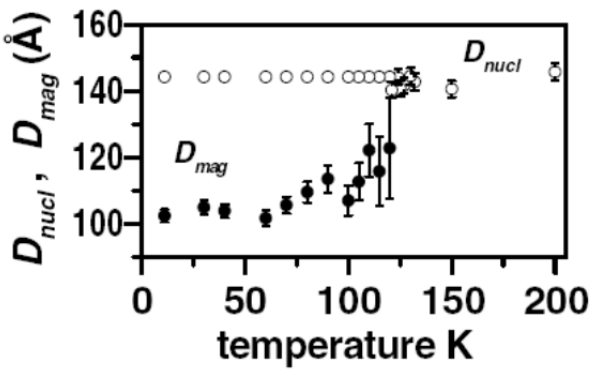

Fig. 2. Temperature dependencies of the volume-averaged diameters of magnetic (D_{mag}) and nuclear (D_{nucl}) regions, solid and open circles, respectively

The electron spin resonance (ESR) in the MnO inside porous media clearly shows the existence of the local spin ordering [54]. The analysis of the ESR signal from confined MnO shows two signal components, one corresponds to crystallized MnO, while another component is due to MnO in an amorphous state. Such an analysis allows us to investigate the magnetic behaviour of the crystallized and amorphous parts of the embedded MnO separately.

The ESR signal associated with the crystalline MnO within a porous glass shows a behaviour having many similarities to the bulk. However, in contrast to the bulk (compare (a) and (c) panels in Fig. 3), the strong ESR signal due to disordered surface spins is observed below the transition.

Magnetic moments in the different crystallographic positions in maghemite γ-Fe_2O_3. Classical ferrimagnetic iron oxides, in particular, maghemite (γ-Fe_2O_3) are widespread in nature. They have been known since ancient times and are widely applied at present [55]. Neutron diffraction experiments with maghemite show that the oxide incorporated within porous glass has the spinel structure with unoccupied positions, which corresponds to the known structure of maghemite [56].

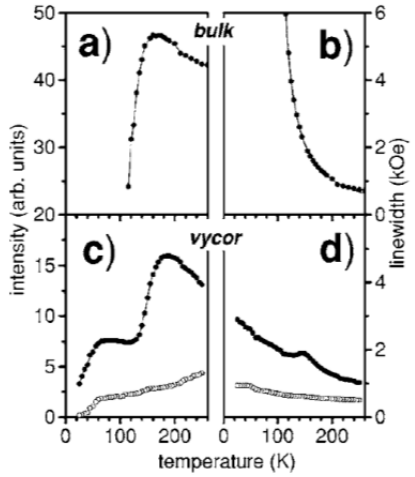

Fig. 3. Intensity (a) and lineshape (b) of the ESR signal from the bulk MnO. Intensity (c) and linewidth (d) of the ESR signal from MnO confined to a porous glass. Open circles correspond to the signal from crystalline MnO and solid circles correspond to the signal from amorphous MnO

The spinel structure contains two types of voids: tetrahedral (eightfold A position) and octahedral (16-fold B position). Magnetic ions can occupy both positions (Fig. 4). Maghemite has the structural formula $(Fe^{3+})[\ Fe^{3+}_{5/6}\square_{1/6}]_2\{O^{2-}\}_4$. In this formula, the parentheses and square brackets refer to the tetrahedral and octahedral voids, respectively, and the symbol □ corresponds to vacancies.

It appears that the magnetic moments in confinement are noticeably different in positions A and B, although Fe^{3+} does not carry the spin moment and the crystal field effect should be negligible. Such an effect was not observed in the bulk and resulted from the size-effect.

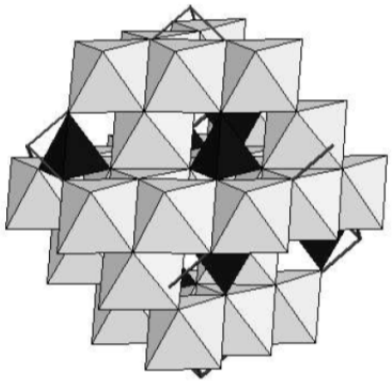

Fig. 4. Crystal structure of spinel with tetrahedral (A) position (in black) and octahedral (B) position (in grey).

Let us consider the nearest environment of the magnetic ions at two positions. The magnetic ion in position A has 4 neighbours in the same positions with the same moment direction and 12 neighbours in position B with the opposite spin direction. The ion in octahedral position B has 6 neighbours with the same spin direction in positions B and 6 neighbours with the opposite spin direction in positions A. Assuming the same spin values in positions A and B, and taking into account the spin directions, the exchange integrals in positions A and B are proportional to $J_A = -12J_{AB} + 4J_{AA}$ and $J_B = -6J_{BA} + 6J_{BB}$, respectively. Substituting the exchange integrals values known for the bulk (we suppose that they are close to those in confinement) maghemite, we obtain J_A/J_B = 2.19. Thus, the moment in position B is bound two times more weakly by the exchange interaction in respect with position A. The more weakly bound spin in position B must evidently be more disordered due to the breaking of local symmetry, and, consequently, its mean value is lower.

The coexistence of two magnetic phases because of the different constant anisotropy on the surface and in the cores of hematite nanoparticles confined to porous glass [57]. The bulk hematite has the corundum crystal structure and presents two-sublattice antiferromagnet with the Néel temperature of 950 K. At 260 K hematite undergoes a spin-reorientation transition, known as the "Morin transition". Below the transition, the moments in two magnetic sub-lattices are exactly antiparallel and aligned along the rhombohedral [111] axis (c-axis in the hexagonal setting) (AF phase). Above the transition, the moments lie in the basal plane (111) with a slight canting resulting in a weak net moment originating from Dzyaloshinskii–Moriya anisotropic super-exchange interaction (WF phase). The spin flip is related to the competition of two terms with different temperature dependencies: the magnetic dipolar interaction and the single-ion anisotropy arising from higher order spin-orbital effects that lead to the different sign of the anisotropy constant.

It turns out that the magnetic contributions into the neutron diffraction patterns in the hematite nanoparticles measured at 300 K and at 10 K are similar. It means that at least down to 10 K there is no any phase transition in confined nanoparticles, in other words, the "Morin transition" is suppressed in the "restricted geometry".

The analysis of the observed intensities of the magnetic reflections shows that they substantially differ from the

intensities, which correspond to the single WF or to the single AF phases. The observed patterns can be equally well described by two models, which are indistinguishable in the frame of the neutron powder diffraction.

The first model assumes that the resulting moment tilts from the rhombohedral axis. The alternative model assumes two magnetic phases: in one phase the magnetic moments are aligned along the rhombohedral axis, as in the bulk hematite below the Morin transition (AF phase), and in the other phase the magnetic moments are confined to the perpendicular plane, as in the bulk hematite above the Morin transition (WF phase).

The data analysis of the neutron diffraction taking into account the results of Mössbauer spectroscopy supports the last model of the two co-existing magnetic phases, corresponding to the phases, which in the bulk hematite exist separately above and below the Morin transition. In the case of nanoparticle one phase exists at the surface, while another one exists in the core, because of the difference in the anisotropy constants.

B. Magnetic Phase Transitions in the "Restricted Geometry"

Continuous transition in the nanostructured nanoparticles. The temperature dependencies of the magnetic moment of the embedded nanoparticles MnO and that in bulk are shown in Fig. 5 [4]. Fitting the observed magnetic moment dependence with a power law $m(T) \sim (1- T/T_N)^{\beta}$ yields the Néel temperature T_N =122.0(2) in contrast with T_N of 117 K in the bulk.

In Fig. 5 it is clearly seen that the discontinuous, first order transition in the bulk becomes continuous in the "restricted geometry". Rigorously, singularities at phase transitions occur in the thermodynamical limit only, when the system is infinite along some directions in space [58]. If the system is finite along all dimensions, it cannot exhibit a singular behaviour. Computer simulation of phase transition in finite-size systems confirms this general conclusion.

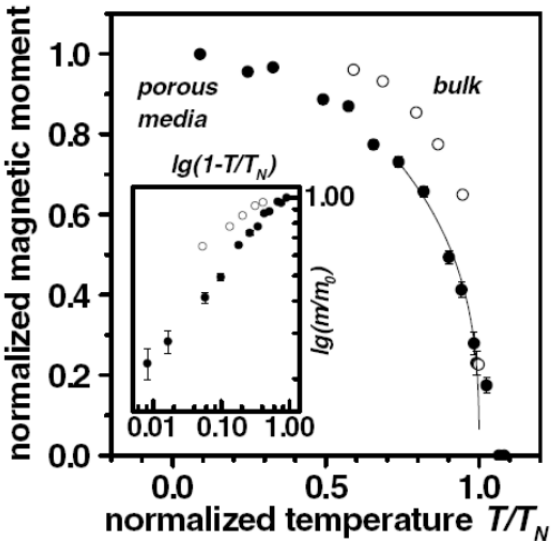

Fig. 5. Temperature dependence of the scaled magnetic moment of MnO embedded in a porous glass (solid circles) and in the bulk MnO (open circles). The solid line corresponds to a fit with a power law. The moment dependencies on a logarithmic scale are shown in the inset.

There is extensive literature, which shows that the continuity and "smoothing" ("rounding") of the phase transition in the "restricted geometry" are general phenomena that follow from the restrictions on the length of the magnetic fluctuations by the size of nanoparticles [59,60].

Indeed, the correlation length ξ when approaching the transition from the above can be described by a power law:

$$\xi(T) = \xi(0)|1 - \frac{T}{T_C(bulk)}|^{\nu},$$

Here η is the so-called critical exponent. In the case of a finite system the $\xi(T)$ at transition temperature T_C is restricted by the characteristic size of nanoparticle L,

$$\xi(T_C) = L = \xi(0)|1 - \frac{T_C}{T_C(bulk)}|^{\nu},$$

It immediately follows that T_C in confinement should be lower than T_C in the bulk:

$$T_C = T_C(bulk)[1 - \frac{\xi(0)}{L}]^{1/\nu}.$$

Really, this law is observed in all known cases (see, for example, confined CoO [61]). However, the nanostructured compounds with Mn^{2+} ion do not obey this law. Probably, it is connected with the specific electronic structure of Mn^{2+}. Up to now there is no clear explanation of this phenomenon.

Evolution of the magnetic phase transition in MnO, nanostructured within the channels of MCM matrices. Unusual behaviour was observed for nanoparticles of MnO nanostructured within the channels of the MCM-41 matrices in the form of thin nanoribbons. In Fig. 6 the temperature dependencies of the normalized magnetic moment for MnO confined to the channels of different diameter are shown. The solid line corresponds to a fit with a power law $m(T) \sim (1- T/T_N)^{\beta}$. Critical exponent β corresponds to the definite theoretical model of the magnetic system. For example, β = 0.5 corresponds to the so-called mean-field theory, when in a three-dimensional system all possible magnetic bonds work.

From neutron and x-ray powder diffraction it follows that the lengths and thinness of the nanoribbons are similar for all matrices. Therefore, the channel diameter is the only characteristic parameter, which defines the dimension of the system. In Fig. 7 the channel dependence of the critical exponent β and T_N is shown. It is seen that with channel decrease the critical exponent β decreases that corresponds to a decrease in the dimensionality of magnetic system. In other words, with channel decrease the system anisotropy increases and magnetic system on nanoparticle becomes more and more close to one-dimensional model.

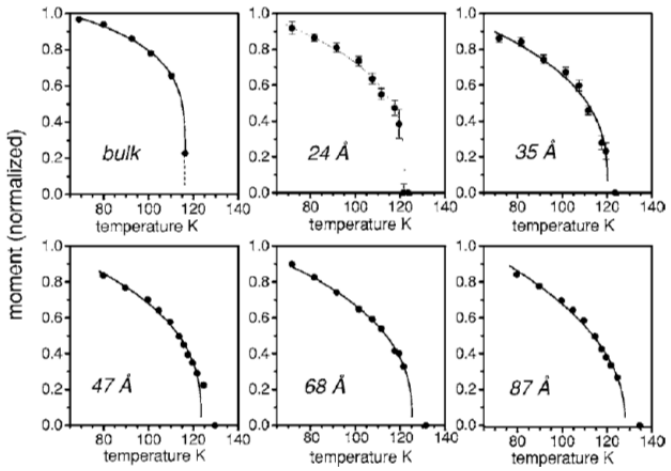

Fig. 6. Temperature dependence of the magnetic moment for MnO confined to the channels of different diameter. The solid line corresponds to a fit with a power law

Nanoparticles confined to the large channels are expected to behave as constrained three-dimensional systems. However, with a decreasing channel diameter, one expects a crossover to one-dimensional behaviour. In this case, the magnetic fluctuations should destroy the long-range magnetic order and T_N should go to zero. However, in our case we see that T_N does not extrapolate to zero with a decreasing channel diameter (Fig. 6).

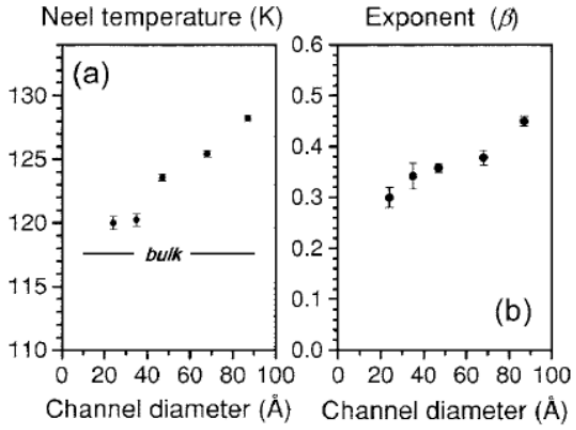

Fig. 7. Dependencies of the Néel temperature T_N (a) and exponent β (b) on channel diameters from the fitting with a power law

C. "Exchange Biased" Magnetic Moment in the "Core-shell" Systems

Such systems present the antiferromagnetic core of MnO with a thin layer of ferrimagnetic γ-Mn_2O_3 [62,63]. Remarkably, while the MnO core is found to have T_N not far from its bulk value (117 K), the magnetic order of the ferrimagnetic shell persists far above T_C (43 K) of the bulk. In Fig. 8 the temperature evolution of the characteristic magnetic reflection is displayed.

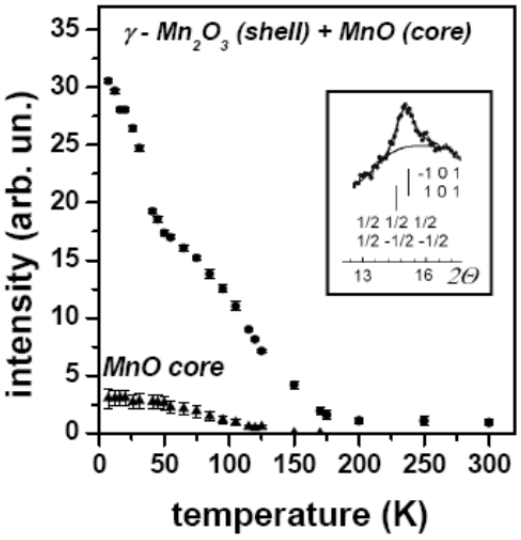

Fig. 8. Temperature dependence of the intensity of the magnetic peak (shown in the insert) with the next contributions from the MnO core: reflections: (1/2,1/2,1/2), (1/2,- 1/2,-1/2) and from the γ-Mn_2O_3 shell: reflections (1,0,1) and (- 1,0,1). The contribution from the MnO core calculated from the profile analysis is shown by triangles

The magnetic signal, which is proportional to square of the ferrimagnetic moment observed above T_N and T_C, up to the room temperature, is clearly seen.

We attribute the observed stable magnetic moment in the ferrimagnetic γ-Mn_2O_3 shell to the exchange coupling between the antiferromagnetic MnO core and the ferrimagnetic shell, as has been observed in the film layered systems. This phenomenon should be considered a proximity effect, when the net ferromagnetic moment due to local violation at the surface (interface) of antiferromagnetic core biases the ferrimagnetic constituent.

III. Ferroelectrics in a Restricted Geometry

For NCMs with embedded ferroelectrics, very interesting and sometimes surprising results have been obtained in recent years. In particular, the dielectric measurements of $NaNO_2$, KH_2PO_4 (KDP), KD_2PO_4 (DKDP), Roshelle salt, KNO_3 within porous glasses and artificial opals have shown the unexpected growth of the real and imaginary parts of the dielectric susceptibility ε above the temperature T_C of the ferroelectric PT [7-9, 27, 44, 64]. In such a situation, an increase in the imaginary part of ε could be attributed to the appearance of conductivity, but in this case the microscopic origin of such conductivity was absolutely unclear. The most remarkable result was the giant growth of ε (up to 10^8 at 100 Hz) upon approaching the bulk melting temperature that was observed for $NaNO_2$ embedded in artificial opals.

These experimental results were the starting point for a detailed study of the temperature evolution of structure of confined $NaNO_2$. To understand the microscopic nature of the observed giant growth of dielectric permittivity in the paraelectric phase we have performed the complex study of structure and properties of these NCMs, including neutron scattering, measurements of heat capacity, NMR, small angle neutron scattering (SANS), dielectric measurements, etc.

A. Samples

Sodium nitrite belongs to the order-disorder ferroelectrics and undergoes the first order phase transition at $T_C \approx 437$ K. At room temperature (RT) $NaNO_2$ has a body centred orthorhombic lattice (a = 3.57 Å, b = 5.578 Å, c = 5.39 Å) with two molecules per unit cell, and its space group is ***Im2m***. In the low-temperature ferroelectric phase, the spontaneous polarization points along the b-axis and appears due to a partial alignment of NO_2 groups along this axis, accompanied by the displacement of sodium ions. At high temperature (above T_C) a mirror plane perpendicular to the b-axis appears and the space group changes to ***Immm***. Bulk sodium nitrite melts at 554.1 K.

KDP and medium deuterated DKDP have a tetragonal structure at the ambient temperature and undergo a phase transition at about 123 K to ferroelectric phase with space group (SG) Fdd2. The high-deuterated DKDP undergoes the ferroelectric phase at 223 K. In the bulk KNO3 crystals the ferroelectric phase is observed only when cooling at atmospheric pressure in the temperature range from 383 K to 398 K.

As porous matrices we used porous glasses with average pore diameters of 320±20, 46±5, 20±3, 7±1 and 3±0.5 nm, artificial opals and chrysotile asbestos with an average diameter of channel of 6±1 nm. The samples with nanostructured $NaNO_2$ and KNO_3 were produced by the immersion of empty vacuum dried porous glasses in the melted $NaNO_2$ (or KNO_3) for several hours. Due to a high wetting ability, these salts penetrate the pores and fill about 22–25% of total sample volume. KDP, DKDP and Rochelle salt were prepared from water solutions of salts. The filling in this case was about 10% of total sample volume.

B. Dielectric Data

In Fig. 9 the temperature dependencies of real ε' and imaginary part ε'' of dielectric permittivity of NCMs with $NaNO_2$ embedded into 7 nm porous glasses are presented.

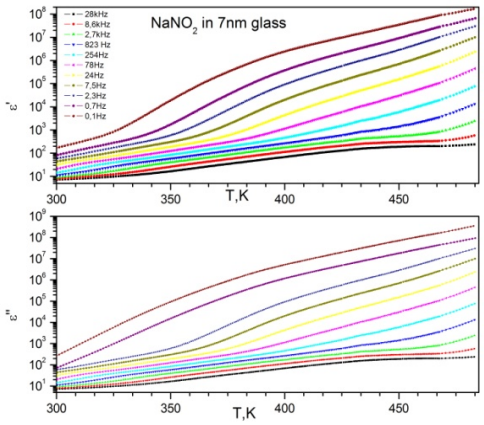

Fig. 9 Temperature dependencies of real ε' and imaginary ε'' parts of dielectric response for $NaNO_2$ within 7 nm porous glasses at different frequencies

At low frequencies, the exponential growth of ε is observed. At 0.1 Hz, the value of ε' achieves 10^8 at 490 K, but we have not observed the peak corresponding to the ferroelectric PT in the dependencies ε(T). It links with great growth of conductivity in the vicinity of PT due to high mobility of sodium ions approaching (and above) T_C. The anomalies at T_C are observed on dependency dε''/dT only. From the analysis of dispersion curves we have determined the parameters of relaxation phenomena and the value of DC (direct current) conductivity **σ**(T) of NCM. This dependency corresponds to the Arrhenius law with activation energy of ~ 1 eV.

C. Structure Evolution and Phase Transitions

The diffraction patterns at 300 K, 420 K (below T_C) and 460 K (above T_C) for sodium nitrite within 7 nm glasses are presented in Fig. 10.

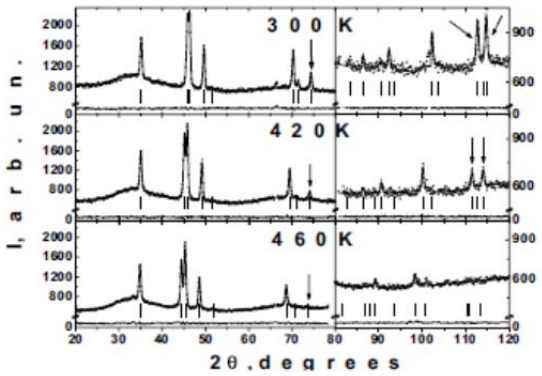

Fig. 10. Neutron diffraction patterns at 300 K, 420 K and 460 K. The arrows indicate the positions of (022), (132) and (123) Bragg peaks in the ferroelectric phase

At all temperatures, the structure of embedded sodium nitrite corresponds to the orthorhombic structure of the bulk $NaNO_2$, but in addition to normal diffraction peaks a diffuse background is also observed due to scattering on porous silica glass. The widths of the observed diffraction peaks are larger than the instrumental resolution, but clearly smaller than the value expected for scattering on isolated 7 nm particles. The average size (≈45 nm) of clusters was determined from the structure refinement and was found to be practically temperature independent up to 460 K. Heating through T_C results in the decrease in intensity of most of the peaks at large scattering angles 2θ, *i.e.*, at large **h k l**, and this effect is much stronger than in the bulk material. Above 523 K, we did not observe any diffraction peaks corresponding to the sodium nitrite structure, *i.e.*, nanocomposite $NaNO_2$ melted entirely below the bulk T_{melt}.

In the case of $NaNO_2$, there are two principal distinguishing groups of Bragg peaks: the intensity of diffraction peaks is proportional to

$$|F|^2 = F^2_{real} + \eta^2(T) \times F^2_{im},$$

where $\mathbf{F}_{real}$ and $\mathbf{F}_{im}$ are the real and imaginary parts of the structure factor F, and η is the order parameter for the ferroelectric phase. For sodium nitrite, there are two families of reflections with different dependencies on η: the first ones, where $\mathbf{F_{im}} \sim 0$ or $\mathbf{F^2_{im}} << \mathbf{F^2_{real}}$ (for example (110), (011), (101) and (200)), are independent from the order parameter, and the second ones (the part of them marked by arrows in Fig.10), where $\mathbf{F^2_{im}} >> \mathbf{F^2_{real}}$ ((022), (123), (132)). The values of $\mathbf{F^2_{im}}$

and $\mathbf{F^2_{real}}$ for different reflections in the ferroelectric phase are presented in Table 1.

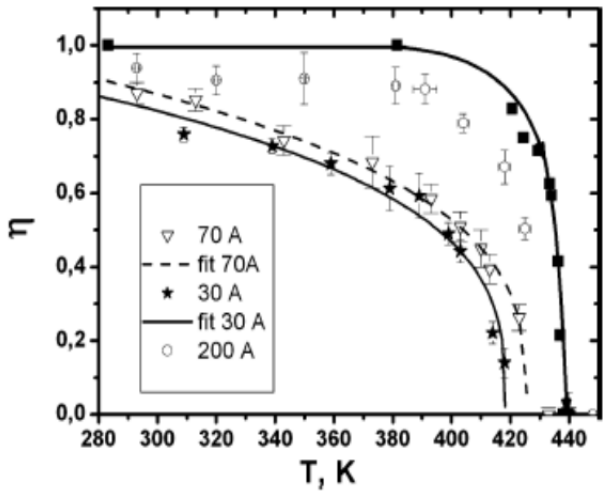

Fig. 11. Temperature dependencies of the order parameter for the bulk (black squares) [65] and NaNO2 embedded into porous glasses with average pore diameters 30 Å (stars), 70 Å (open triangles) and 200 Å (open circles)

TABLE 1

REAL AND IMAGINARY PARTS OF THE STRUCTURE FACTOR FOR SODIUM NITRITE IN THE FERROELECTRIC PHASE FOR DIFFERENT REFLECTIONS

H	K	L	F^2_{real}	F^2_{im}
0	1	1	2.83	0.02
1	1	0	6.74	0.07
1	0	1	8.17	0
2	0	0	8.18	0
0	2	0	10.82	0.009
1	1	2	0.006	0.687
0	2	2	0.254	3.864
0	1	3	0.01	1.065
1	3	0	0.36	0.266
2	2	0	3.81	0.054
1	3	2	0.054	2.762
1	2	3	0.3	2.718
0	4	2	0.028	5.128

It is easy to see that the intensities of these peaks are practically proportional to $\boldsymbol{\eta^2}$. The curves $\boldsymbol{\eta}$(T) for NCM (Fig. 11) can be well fitted by a power law $\boldsymbol{(1- T/T_C)^{\beta}}$ with T_C=418.5±3.5 and 423.6±2.1 K for the 3 and 7 nm porous glasses, respectively. The critical exponent β is equal to 0.33±0.04 for both NCMs. This value of β is in a good agreement with the value (0.362±0.004) obtained for the 3D-Ising model [66], by computer simulation of finite-size scaling for a second order PT. The curve $\boldsymbol{\eta}$(T) for NCM for the 20 nm porous glass differs principally from those for nanocomposites with 3 and 7 nm pores and looks similar to the dependence obtained for the bulk [65]. The crossover of PT for small nanoparticles from the first order to the second order was confirmed by measurements of heat capacity [67].

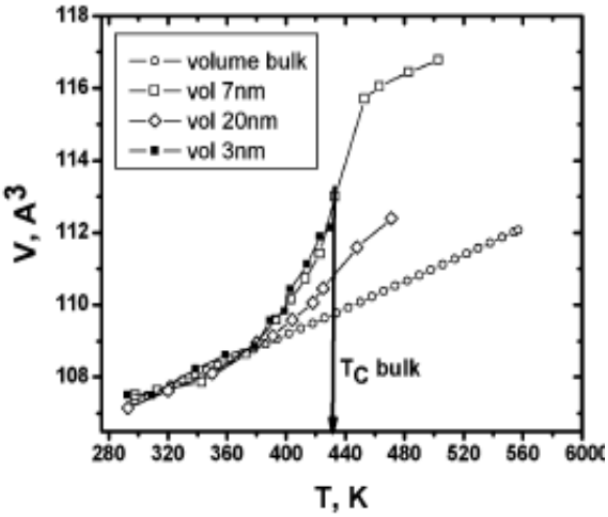

Fig. 12. Temperature dependencies of the unit cell volume for 3 nm (black squares), 7 nm (open squares) and 20 nm (open rhombuses) porous glasses and the massive sodium nitrite

In Fig. 12 the temperature dependencies of the unit cell volume for all types of NCMs and for the bulk are presented. These curves for NCM are visibly different from that for the bulk. The appearance of the fast increase in the volume for all NCMs is observed at ~380 K, i.e., below T_C, and at high temperature these values exceed the unit cell volume of bulk sodium nitrite in the vicinity of the melting point. Such behaviour can be considered evidence of lattice "softening" in NCM with 3 and 20 nm pores as it has been proven earlier for sodium nitrite within 7 nm glasses. This essential increase in unit cell volume of ~8 % (and a decrease in density) must lead to a visible change of contrast at SANS. Indeed, it is easy to see in Fig. 13 that upon heating throughout T_C (~164 C) the contrast changes approximately1.5 times at Q ≈ 0.018 $Å^{-1}$.

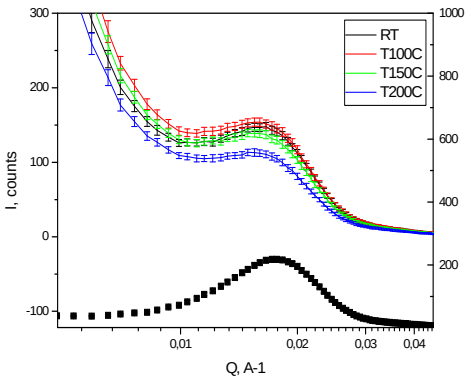

Fig. 13. Temperature dependencies of intensity of SANS for $NaNO_2$ within 7 nm porous glasses. Black line corresponds to scattering on empty porous glasses

D. Thermal Vibrations and Pre-melted State

The analysis of neutron diffraction patterns enables us to obtain information concerning the thermal motions of constituent ions of sodium nitrite within porous matrices.

The results at 420 K (below *Tc*) and 460 K (above *Tc*) are presented as ellipsoids of 50% probability in Fig. 14 and as ellipsoids of 5% probability in Fig. 15 (since oxygen thermal displacements are very large for a porous sample). For the bulk material, these ellipsoids are close to a sphere at all temperatures, and the amplitudes of thermal motion do not change practically upon heating throughout T_C. For confined sodium nitrite below T_C, these ellipsoids are clearly anisotropic and slightly larger than for the bulk, but upon heating through T_C the picture changes drastically.

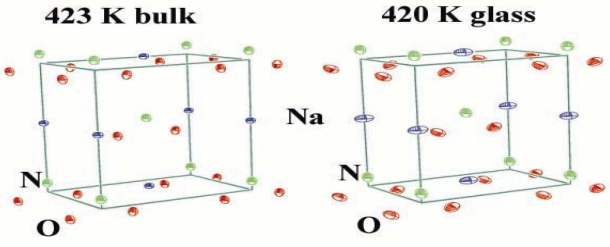

Fig. 14. Ellipsoids of thermal motions for the bulk (left) and confined within 7 nm porous glasses (right) $NaNO_2$ below T_C

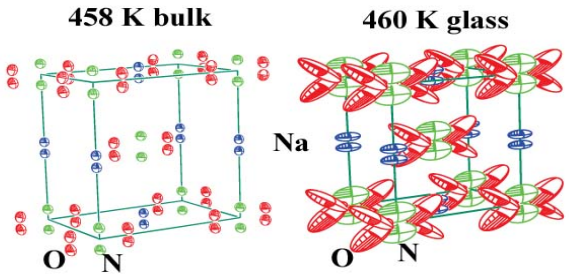

Fig. 15. Ellipsoids of thermal motions for the bulk (left) and confined within 7 nm porous glasses (right) $NaNO_2$ above T_C

In the paraelectric phase (above *Tc*), the vibrations of Na and N form practically the flat disks perpendicular to the ***b*** direction for Na and the ***a*** direction for N as a result of mixed rotation around the ***a*** and ***c*** axes, while oxygen ions form very stretched ellipsoids predominantly along the ***a*** and ***c*** directions, as should be expected at increasing rotation around the ***b*** axis. The values of oxygen thermal displacements along the ***c*** and ***a*** directions at 460 K (above T_C) are equal to 1.21 and 0.93 E, respectively [i.e., more than 25% of O-O (3.34 E) distance for neighbouring NO_2 groups]. These values essentially exceed the Lindemann criterion for melting. This experimental fact (and the sharp growth of unit cell volume upon heating through T_C) allows concluding that above T_C and up to melting (~525 K) a specific volume pre-melted state with high mobility of constituent ions forms in confined sodium nitrite more than 100 K below the bulk T_{melt}. It is necessary to underline that this pre-melted state is not related to the spreading surface (we have observed the diffraction peaks essentially above T_C), but it has a volume character and probably originates from some size effect of yet unclear nature. Measurements of NMR on ^{23}Na isotope confirm the growth (approximately twentyfold) of sodium mobility in this NCM upon heating [68].

E. Size Effect and Metastable Phases

The neutron diffraction patterns for high-deuterated DKDP show strong broadening of Bragg reflections due to size-effect leading to large peak overlapping. Surprisingly, the measured patterns at all temperatures appear to be inconsistent with the profiles simulated in the orthorhombic $Fdd2$ and tetragonal $I\bar{4}2d$ space groups (SG). From the comparison of the obtained diffraction patterns with the simulated ones, calculated for different crystal structures reported for DKDP (KDP) (see Table 1), it follows that the observed patterns can be best fitted by the monoclinic crystal structure with SG $P2_1$ and the unit-cell parameters close to reported in [69] for high-deuterated DKDP. Unfortunately, the hydrogen positions for this monoclinic structure are unknown. Moreover, due to low symmetry and strong peak overlapping it is impossible to refine these positions from our data. Therefore, we have refined the average diameter (size) of the embedded nanoparticles and the unit-cell parameters only in the so-called "matching mode" by the FULLPROF program. The temperature dependencies of these parameters are shown in Fig. 16 and there is no any anomalies in the temperature interval of 90–308 K, i.e., the ferroelectric phase transition is absent in this temperature span for confined DKDP.

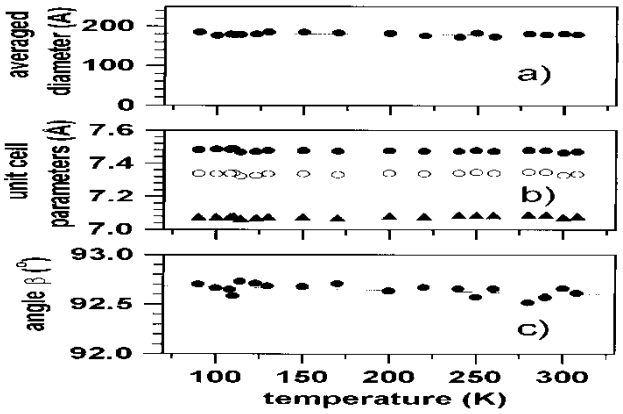

Fig. 16. Temperature dependencies of refined average diameter of nanoparticle (a); unit cell parameters for monoclinic cell (b): **a** (solid circles), **b/2** (open circles) and **c** (triangles); monoclinic angle β (c) for high-deuterated DKDP embedded into 7 nm porous glasses.

It is shown that the monoclinic modification of the high-deuterated $K(D_{1-x}H_x)_2PO_4$ can exist at room temperature [70,71] and crystallize from the high-deuterated (≈ 98%) aqueous solution only [70], but at ambient conditions this modification transforms into the tetragonal form in a few days [71]. Our samples with DKDP were also crystallized from the aqueous solution and prepared some months before the experiment and stored at ambient conditions; therefore, the stability of the observed monoclinic phase was surprising. It is possible that such stability is associated with the size-effect and/or with characteristics of interaction of DKDP with a porous matrix.

Some years ago it was shown that thin films of KNO_3 exhibit ferroelectric properties at room temperature [72]. One of the simple ways of producing nano-sized ferroelectrics is to introduce them into the porous glass matrices. As it is shown

in the paper [64] for KNO_3 embedded into porous glasses an increase in a pore diameter from 320 nm to 46 nm leads to an extended temperature range, where the metastable ferroelectric phase exits. In Fig. 17 the temperature dependencies of e' upon heating and cooling for KNO_3 embedded into 320, 46 and 7 nm porous glasses are presented. It is easy to see that an increase in nanoparticle size leads to smearing of PT and an increase in thermal hysteresis. For NCM with 7 nm pores a sharp growth of e' due to melting of potassium nitrate within pores is observed and T_{melt} in this case is essentially smaller than in the bulk (600 K).

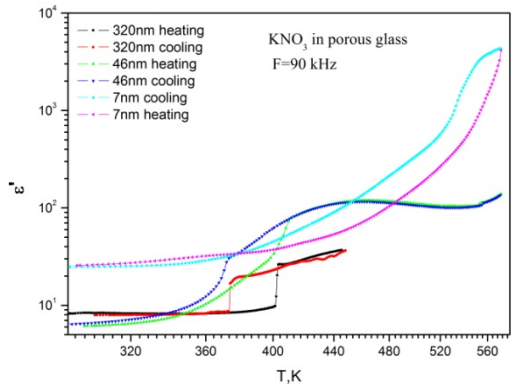

Fig. 17. Temperature dependencies of real part of dielectric permittivity for KNO_3 within various porous glasses upon cooling and heating

IV. Conclusions

We have studied the physical properties and crystal structure of various ferroelectric and magnetic NCMs on the basis of porous matrices with a different average pore diameter and, therefore, we can define some common features of these materials:

1. Embedding from wetting melt and chemical embedding produce non-spherical clusters with an average diameter larger than the pore diameter.
2. For some NCMs there is the critical size of nanoparticles when the crossover of PT type is observed.
3. Examined ferroelectric NCMs with small particles demonstrate the giant dielectric permittivity in the paraelectric phase.
4. A new volume pre-melted state with extremely large thermal motions of constituent ions has been recovered for sodium nitrite.
5. The confinement can stabilize metastable phases.

Acknowledgements

The research at SPbSPU has been supported by the Federal Program “Research and Development in Priority Development Areas of Scientific and Technological Complex of Russia in 2007–2013”, Federal Program “Research and Scientific and Pedagogical Personnel of Innovative Russia in 2009–2013” and by a grant of the Government of St. Petersburg.

References

1. **W.L. Zhong, Y.G. Wang, P.L. Zhang,** Ferroelectric Lett. **1** (1998) 131 and references therein.
2. **W.Neubeck, L. Ranno, M. Hunt, C. Vettier, D. Givord**, Appl.Surf.Sci. **138–139** (1999) 195.
3. **S. Li, J.A. Eastman, Z. Li, C.M. Foster, R.E. Newnham, L.E. Cross**, Phys. Lett. **A 212** (1996) 341.
4. **I.V. Golosovsky, I. Mirebeau, G. Andrй, D.A. Kurdyukov, Yu.A. Kumzerov, S.B. Vakhrushev**, Phys. Rev. Lett.**86** (2001) 5783.
5. **P. Sheng, R.W. Cohen, J.R. Schrieffer,** J. Phys. C: Solid State Phys.**14** (1981) L565.
6. **Yu.A. Kumzerov, A.A. Nabereznov, S.B. Vakhrushev, B.N. Savenko,** Phys. Rev. **B 52** (1995) 4772.
7. **S.V. Pankova, V.V. Poborchii, V.G. Solovev**, J. Phys.: Condens.Matter **8** (1996) L203.
8. **E.V. Colla, A.V. Fokin, Yu.A. Kumzerov**, Solid State Commun.**103** (1997) 127.
9. **E.V. Colla, E.Yu. Koroleva, Yu.A. Kumzerov, B.N. Savenko** Ferroelectr. Lett. **20 (**1996) 143
10. **A. Beskrovny, I. Golosovsky, A. Fokin, Yu. Kumzerov, A. Kurbakov, A. Naberezhnov, S. Vakhrushev**, Appl. Phys. **A 74** (2002) S1001.
11. **A.V. Fokin, Yu.A. Kumzerov, N.M. Okuneva, A.A. Naberezhnov, S.B. Vakhrushev, I.V. Golosovsky,A.I. Kurbakov**, Phys. Rev. Lett. **89** (2002) 175503-1.
12. **E.V. Charnaya, T.Loeser, D.Michel, C.Tien, D.Yaskov, Yu.A. Kumzerov**, Phys. Rev. Lett. **88** (2001) 097602-1.
13. **J.M. Drake, G.S. Grest, J. Klafter, R. Kopelman** (Eds.), Dynamics in Small Confining Systems, MRS, Warrendale,PA, 1999.
14. **M. J. Graf, T. E. Huber, and C. A. Huber**, Phys. Rev. **B 45**, (1992) 3133.
15. **E.V. Charnaya, C. Tien, K. J. Lin, C. S. Wur, and Yu. A. Kumzerov**, Phys. Rev. **B 58**, (1998) 467
16. **G. Kh. Panova , A. A. Naberezhnov, A. V. Fokin**, Physics of the Solid State,**50(7),** (2008) 1370
17. **M. H.W. Chan, K. I. Blum, S.Q. Murphy, G. K. S. Wong, J. D. Reppy**, Phys. Rev. Lett. **61**, (1988) 1950
18. **M. Larson, N. Mulders, G. Ahlers**, Phys. Rev. Lett. **68**, (1992) 3896
19. **R. Mu, V.M. Malhotra**, Phys. Rev. B **44**, 4296 (1991).
20. **J. A. Duffy, N. J. Wilkinson, H.M. Fretwell, M. A. Alam,** J. Phys. Condens. Matter **7**, (1995), L27 and references therein.
21. **C. L. Jackson, G. B. McKenna,** J. Chem. Phys. **93**, (1990) 9002
22. **J. R. Beamish, A. Hikata, L. Tell, C. Elbaum**, Phys.Rev. Lett. **50**, (1983) 425
23. B**. F. Borisov, E.V. Charnaya, P.G. Plotnikov, W.-D. Hoffmann, D. Michel, Yu. A. Kumzerov, C. Tien, C. S.Wur**, Phys. Rev. B **58**, (1998) 5329
24. **M.-C. Bellissent-Funel, J. Lal, L. Bosio,** J. Chem. Phys. **98**, (1993) 4246
25. **T. Kanata, T. Yoshikawa, K. Kubota**, Solid State Commun. **62**, (1987) 765
26. **K. Ishikawa, K. Yoshikawa, N. Okada**, Phys. Rev. B **37**, (1988) 5852
27. **E.V. Colla, A.V. Fokin, E.Yu. Koroleva, Yu. A. Kumzerov, S. B. Vakhrushev, B. N. Savenko**, Nanostruct. Mater. **12**, (1999) 963
28. **K. Anliker, H. R. Brugger, W. Kдnzig**, Helv. Phys.Acta **27**, (1954) 99
29. **K. Saegusa,W. E. Rhine, H. K. Bowen**, J. Am. Ceram. Soc. **76**, (1993) 1505
30. **K. Uchino, E. Sadanaga, T. Hirose,** J. Am. Ceram. Soc. **72**, (1989) 1555
31. **P. Marquardt, H. Gleiter**, Phys. Rev. Lett. **48**, (1982) 1423
32. **W. L. Zhong, Y.G. Wang, P. L. Zhang**, Phys. Lett. **A 189**, (1994) .121
33. **W. Buchheit, U. Kreibig, D. Mьller, A.Voigt**, Z. Phys. **B 32**, (1978) 83
34. **S.B. Vakhrushev, Yu. A. Kumzerov, A. Fokin, A.A. Naberezhnov, B. Zalar, A. Lebar, R. Blinc**, Phys. Rev **B70**, (2004) 132102(3)
35. **D.C. Steytler, J.C. Dore, C. J.Wright**, J. Phys. Chem.**87**, (1983) 2458
36. **P. Wiltzius, F. S. Bates, S. B. Dierker, G. D. Wignall**, Phys. Rev. **A 36**, (1987) 2991
37. **E Yu Koroleva, D Nuzhnyy, J Pokorny, S Kamba, Yu A Kumzerov, S B Vakhrushev, J Petzelt** Nanotechnology **20** (2009) 395706 (7)
38. **K. Saegusa,W. E. Rhine, H. K. Bowen,** J. Am. Ceram. Soc. **76**, (1993) 1505
39. **E.V. Colla, A.V. Fokin, E.Yu. Koroleva, Yu. A. Kumzerov, S. B. Vakhrushev, B. N. Savenko**, Nanostruct. Mater. **12**, (1999) 963
40. **D.C. Steytler, J.C. Dore, C. J.Wright**, J. Phys. Chem. **87**, (1983) 2458
41. **J. C. Dore, M. Dunn, and P. Chieux,** J. Phys. (Paris), Colloq. **48**, (1987) C1-457
42. **M. J. Benham, J.C. Cook, J.-C. Li, D. K. Ross, P. L. Hall, B. Sarkissian**, Phys. Rev**. B 39**, (1989) 633
43. **P. Wiltzius, F. S. Bates, S. B. Dierker, G. D. Wignall**, Phys. Rev. **A 36**, (1987) 2991

44. **B. Dorner, I. Golosovsky, Yu. Kumzerov, D. Kurdyukov, A. Naberezhnov, A. Sotnikov, S. Vakhrushev**, Ferroelectrics **286**, (2003) 213
45. **A. Naberezhnov, A. Fokin, Yu. Kumzerov , A. Sotnikov , S. Vakhrushev, B. Dorner**, Eur. Phys. J. **E 12**, (2003) s21
46. **I.V. Golosovsky, R.G. Delaplane, A.A. Naberezhnov, Y.A. Kumzerov**, Phys. Rev. **B69**, (2004) 132301(4)
47. **I.V. Golosovsky, I. Mirebeau, E. Elkaim, D.A. Kurdyukov, Y.A. Kumzerov** Eur. Phys. J**. B 47**, (2005) 55
48. I**.V. Golosovsky, G. Salazar-Alvarez, A. López-Ortega, M. A. González, J. Sort, M. Estrader, S. Suriñach, M. D. Baró, J. Nogués** Phys.Rev. Lett. 102, (2009) 247201
49. **P. Marquardt, H. Gleiter,** Phys. Rev. Lett. **48**, (1982) 1423
50. **C. G. Shull, W. A. Strauser, E. O. Wollan,** Phys. Rev.**83**, (1951) 333
51. **W. L. Roth**, Phys. Rev. **110**, (1958) 1333
52. **M. E. Lines, E. D. Jones**, Phys. Rev. **139**, (1965) A1313
53. **D. S. Rodbell, J. Owen**. J. Appl. Phys., **35**, (1964) 1002
54. **I. V. Golosovsky, D. Arcon, P. Cevc, Z. Jaglicic, V. P. Sakhnenko, D. A. Kurdyukov, Yu. A. Kumzerov**, Phys. Rev. **B72**, (2005) 144410
55. **R. Dronskowski**, Adv. Funct. Mater. **11**, (2001) 27
56. **I. V. Golosovsky, M. Tovar, U. Hoffman, I. Mirebeau, F. Fauth, D. A. Kurdyukov, Yu. A. Kumzerov**, JETP Letters, **83**, (2006) 298
57. **I. V. Golosovsky, I. Mirebeau, F. Fauth, D. A. Kurdyukov, Yu. A. Kumzerov**, Solid State Communications, **141,** (2007) 178
58. **G. Cabrera**, Int. J. Mod. Phys. B **4**, (1990) 1671
59. **K. Binder, D. P. Landau**, Phys. Rev. B**30**, (1984) 1477
60. **M. N. Barber,** "Phase Transitions and Critical Phenomena" vol. 8, ed. C. Domb and L. Lebowitz, (New York: Academic), 145, (1983).
61. **I. V. Golosovsky, I. Mirebeau, G. André, M. Tovar, D. M. Tobbens, D. A. Kurdyukov, Yu. A. Kumzerov**, Physics of the Solid State, **48**, (2006) 2130
62. **G. Salazar-Alvarez, J. Sort, S. Suriñach, M. Baró, J. Nogués**, J. Am. Chem. Soc. **129**, (2007) 9102
63. **A. E. Berkowitz, G. F. Rodriguez, J. I. Hong, K. An, T. Hyeon, N. Agarwal, D. J. Smith, E. E. Fullerton**, Phys. Rev. B**77**, (2008) 024403
64. **R. Poprawski, E. Rysiakiewicz-Pasek, A. Sieradzki, A. Ciźman, J. Polańska,** Journal of Non-Crystalline Solids 353 (2007) 4457–4461
65. **A. da Costa Lamas, S.-L. Chang, S. Caticha-Ellis**, Phys. Status Solidi(a) 68, (1981) 173
66. **D.P. Landau, J. Magn**. Magn. Mater. 200, (1999) 231
67. **Z. Kutnjak, B. Vodopivec, R. Blinc, A.V. Fokin, Yu. A. Kumzerov, S.B. Vakhrushev** J. Chem. Phys. **123**, (2005) 084708
68. **S. B. Vakhrushev, Yu. A. Kumzerov, A. Fokin, A. A. Naberezhnov, B. Zalar, A. Lebar, R. Blinc** Phys. Rev. B **70**, (2004) 132102
69. **R. Nelmes**, Phys. Stat. Sol. (b) **52, (**1972) K89
70. **K. Itoh, T. Matsubayashi, E. Nakamura H. Motegi**, J. Phys. Soc. Japan **39**, (1975) 843
71. **M. Mathew, W. Wong-Ng**, J. Sol. State Chem. **114,** (1995) 219
72. **J.F. Scott, H.M. Duiker, P.D. Beale, B. Pouligny, K. Dimmler, M. Parris, D. Butler, S. Eaton**, Physica B 150 (1988) 160

Alexey Filimonov, born on 16 April 1967. In 1974 he received his M.Sc. in Physics from Leningrad Polytechnical Institute. In 2000 he obtained a Doctoral Degree in Physics and Mathematics.
Employment: 1992 – present, St. Petersburg State Polytechnical University, Associated Professor, Director of the **Research and Educational Centre "Physics of Nanocomposite Materials".** Recent publications: R.G. Burkovsky, Yu.A. Bronwald, A.V. Filimonov, A.I. Rudskoy, D. Chernyshov, A. Bosak, J. Hlinka, X. Long, Z.-G. Ye, and S.B. Vakhrushev "Structural Heterogeneity and Diffuse Scattering in Morphotropic Lead Zirconate-Titanate Single Crystals" Physical Review Letters. – 2012. – Vol. 109. – p. 097603; R.G. Burkovsky, A.V. Filimonov, A.I. Rudskoy, K. Hirota, M. Matsuura, S.B. Vakhrushev. "Diffuse Scattering Anisotropy and Inhomogeneous Lattice Deformations in Lead Magnoniobate Relaxor above the Burns Temperature" Phys. Rev. B 85, 094108 (2012); M.C. Wurz, A. Shaganov, L. Rissing, A. Filimonov, S. Vakhrushev "Investigation of the Crystallization of NiFe81/19 Depending on the Annealing Temperature" Magnetic Materials, Processes and Devices – 2012.- Vol. 50, N 10. - **p. 147–156**
Alexey Filimonov is a member of DAAD – Alumni.
E-mail: filimonov@rphf.spbstu.ru

Andrey Rudskoy, graduated from Leningrad Polytechnical Institute in 1981 and in 1993 graduated from the Academy of National Economy under the Government of the Russian Federation. He received his degree of Doctor of Engineering Sciences (Advanced Doctorship Degree) in 1998. In 2008 he became a Corresponding Member of the Russian Academy of Sciences.
Since 1985 he has been a Professor. Since 2001 he has been the Chair of the Department of Metal Forming of St. Petersburg State Polytechnical University. Since 2003 he has been the SPbSPU Vice-rector of the Polytechnical University. Since 2007 Andrey I. Rudskoy is the Scientific Director of SPbSPU Scientific-innovative Institute of Materials and Technology. In May, 2011, according to the decision of the academic staff of Polytechnical University, he was appointed the Rector of SPbSPU.
The area of scientific interests of Andrey I. Rudskoy covers the theory and technology of nano-structured metallic materials, the theory of the metal forming and powdered materials. He is the author of more than 160 scientific papers, 9 monographs and 5 patents. A.I. Rudskoy is a member of the Russian Academy of Engineering, associate member of an International Higher Education Academy of Sciences, a member of the European Union of Metallurgists, a professor-adviser of Planck Institute and University of Hannover (Germany).

Aleksandr Naberezhnov, born on 13 April 1951. In 1974 he received his M.Sc. in Physics from Leningrad Polytechnical Institute. In 1996 he obtained a Doctoral Degree in Physics and Mathematics.
Employment: 1974–1985, Leningrad Nuclear Physics Institute; 1985 – present, Ioffe Institute, **Senior Scientist**; 2008 – present, St.Petersburg State Polytechnical University, **Senior Scientist.** Recent publications: A.A. Shikov, G.K. Panova, M.G. Zemlyanov, P.P. Parshin, Y.A. Kumzerov, A.A. Naberezhnov, D.S. Shaitura "Low-temperature Vibrational Properties of Tin Nanoparticles in Porous Glass" Phys. of the Solid State, 53(12), 2515-2519 (2011); I.I. Popov, R.R. Nigmatullin, E.Yu. Koroleva, A.A. Nabereznov "The Generalized Jonscher's Relationship for Conductivity and Its Confirmation for Porous Structures" Journal of Non-Crystalline Solids 358 1–7 (2012); T.V. Antropova, I.N. Anfimova, I.V. Golosovsky, Yu.A. Kibalin, A.A. Naberezhnov, N.I. Porechnaya, O.A. Pshenko and A.V. Filimonov "Structure of Magnetic Nanoclusters in Ferriferous Alkali Borosilicate Glasses" Physics of the Solid State, 54(10), 2106–2111, (2012).
Aleksandr Naberezhnov is a member of: Russian Neutron Scattering Society, Neutron Scattering Society of America (NSSA) (since 1993) and Schweizerische Gesellschaft für Neutronenstreuung (Société Suisse pour la Diffusion des Neutrons) SGN/SSDN, Switzerland (since 1998).

Sergey Vakhrushev Educational background: (1975) – M.Sc. in Radiation Chemistry; (1986) – Candidate of Sciences (equivalent to PhD) in Solid State Physics; (1998) – Doctor of Sciences (Habilitation) in Solid State Physics, Ioffe Institute RAS.
Work experience: 2004 – present, Professor, Faculty of Radiophysical Science and Engineering, St. Petersburg State Polytechnical University, St. Petersburg, Russia; 1999 – present, Head of Neutron Research Lab, Principal Researcher, Ioffe Institute (PTI), St. Petersburg, Russia. Recent publications: R.G. Burkovsky, Yu.A. Bronwald, A.V. Filimonov, A.I. Rudskoy, D. Chernyshov, A. Bosak, J. Hlinka, X. Long, Z.-G. Ye, and S.B. Vakhrushev "Structural Heterogeneity and Diffuse Scattering in Morphotropic Lead Zirconate-Titanate Single Crystals" *Phys. Rev. Lett*., 117, 097603 (2012); A. Bosak, D. Chernyshov, S. Vakhrushev, M. Krisch "Diffuse Scattering in Relaxor Ferroelectrics: True Three-dimensional Mapping, Experimental Artefacts and Modelling, "*Acta Crystallographica Section A*", 117, 123 (2012); R.G. Burkovsky, A.V. Filimonov, A.I. Rudskoy, K. Hirota, M. Matsuura, S.B. Vakhrushev "Diffuse Scattering Anisotropy and Inhomogeneous Lattice Deformations in the Lead Magnoniobate Relaxor PMN above the Burns Temperature" *Phys. Rev*. **B 85**, 094108 (2012).
Fields of interest: structural phase transitions and critical phenomena; nanocomposite materials based on porous matrices; neutron and X-ray inelastic and diffuse scattering; structural ordering and disordering in the mixed crystals.
Sergey Vakhrushev is the Vice President of Russian Neutronographic Society; Vice Chairman of the Scientific Council of Neutron Physics of the Russian Academy of Sciences; Delegate of Russia in the European Neutron Scattering Association; Member of the Presidium of the Scientific Council on Physics of Ferroelectrics and Dielectrics of the Russian Academy of Sciences; Member of Steering Committee of European Meetings on Ferroelectricity; Member of ECAPD International Advisory Board; Member of the American Neutron Scattering Society.

Ekaterina Koroleva, born on 29 September 1967. In 1990 she received her M.Sc. in Radiophysics from St. Petersburg State Polytechnical University. In 1998 she obtained a Doctoral Degree in Physics and Mathematics – Ioffe Institute. Major field: solid state physics, Minor fields: dielectric spectroscopy, structural phase transitions, ferroelectrics, nanocomposites.
Employment: 1990 – present, Research Assistant, Junior Researcher, Researcher and SENIOR RESEARCHER (since 2003), Ioffe Institute. 2008 – present, Senior Researcher, St.Petersburg State Polytechnical University. Main publications: E.V. Colla, E.Yu. Koroleva, N.M. Okuneva, S.B. Vakhrushev "Low Frequency Dielectric Response of $PbMg_{1/3}Nb_{2/3}O_3$". - J.Phys.Condens. Matter, **4**, pp. 3671-3677, 1992; E.V. Colla, E.Yu. Koroleva, S.B. Vakhrushev "Long-time Relaxation of the Dielectric Response in Lead Magnoniobate. - Phys.Rev.Lett., v. **74**, No. 9, pp. 1681-1684, 1995; E.Yu. Koroleva, D. Nuzhnyy, J. Pokorny, S. Kamba, Y.A. Kumzerov, S.B. Vakhrushev, J. Petzelt "The Negative Phonon Confinement Effect in Nanoscopic Sodium Nitrite -Nanotechnology, **20**, 39 Art.No: #395706, 2009.

Igor Golosovsky. After graduating from the State University of Nizny Novgorod (Russia) in 1969 up to now he has been working at the Division of Condensed Matter Physics of St. Petersburg Nuclear Physics Institute. In 2007 he received his Doctoral degree, equivalent to the "dr. habilitation" in Europe. Scientific interest covers mainly atomic and magnetic ordering in the different objects: bulk, films and nanostructured systems. The total number of the published papers is 95. The author is a member of the following organizations: the Council of Solid State Physics of the Russian Academy of Sciences, American NanoSociety and Russian Neutron Association. Current projects – magnetic and crystal structures in the mixed multiferroics, nanostructured magnetic "core-shell" oxide systems, antiferromagnetic epitaxial films, atomic vibrations in the low-melting metals nanostructured within porous media.

Yury Kumzerov, Education: 1972 – St. Petersburg State University, Faculty of Physics, Master Degree in Physics; 1978 – Candidate of Sciences, Thesis: "Superconductivity in Ultrathin Wires"; 1987 – Doctor of Sciences, Thesis: "Electronic Properties of Approximately One-dimensional Systems".
Employment: 1972 to present – Ioffe Physical Technical Institute, Russian Academy of Sciences (St. Petersburg, Russia); 1993 to present – DEPUTY DIRECTOR OF DIVISION (Division of Physics of Dielectric and Semiconductors, Ioffe Institute). Previous publications: Yu.A. Kumzerov "Nanostructured Coatings of Inner Surfaces in Microporous Matrixes, G.M. Chow et al. (ed.), Nanostructured Films and Coatings, pp. 63–76, 2000, Kluwer Academic Publishers, Printed in Netherlands; Yu. Kumzerov "Nanostructures within Porous Matrixes, Proceedings of Global Samsung Forum, November 6, 2002, Samsung Advanced Institute of Technology, Kiheung, Kyunggi, South Korea, pp. 64–74; Y.Kumzerov, S.Vakrushev "Nanostructures within Porous Materials, In "Encyclopedia of Nanoscience and Nanotechnology", (H.S. Nalwa Ed.), 2004, American Scientific Publishers, vol. VII, pp. 811–849
Research interests: nanostructures, nanoporous materials, physical properties of materials in confined geometries, phase transitions in restricted geometry, nanowires from metals, semiconductors, insulators.

Aleksejs Fiļimonovs, Andrejs Rudskojs, Aleksandrs Naberežnovs, Sergejs Vahruševs, Jekaterina Koroļova, Igors Golovskis, Jurijs Kumžerovs. Jauni nanokompozītu materiāli uz porainas dielektriskas matricas bāzes
Darbā pētīta mākslīgi ierobežotas ģeometrijas ietekme uz nanokompozītmateriālu makroskopiskajām īpašībām, kristālisko struktūru un fāžu pārejām, kas veidoti uz porainas matricas bāzes ar nanometra izmēru kanāliem, un kā pildvielu satur segnetokeramiskos un magnētiskos materiālus. Kā porainās matricas izmantoti poraini stikli ar vidējo poru diametru 320±20, 46±5, 20±3, 7±1 un 3±0,5 nm, sintētiskie (mākslīgie) opali, hrizotilasbests, matricas SBA-15 ar vidējo poru diametru diapazonā no 47-87 Å un MCM-41 ar poru izmēriem 24 Å, 35 Å, 47 Å, 68 Å un 87 Å. Magnētiskie materiāli – MnO, CoO un Fe_2O_3 tika sintezēti tieši matrices porās, bet segnetoelektriķi porās tika ievadīti no kausējuma ($NaNO_2$, KNO_3) vai ūdens šķīduma (KH_2PO_4 (KDP), KD_2PO_4 (DKDP), segneta sāls). DKDP deiterēšanas pakāpe sasniedza 98%. Pētījumi tika veikti ar neitronu difrakcijas un rentgenstarojuma, maza leņķa neitronu izkliedes, elektronu paramagnētiskās rezonanses un dielektriskās spektroskopijas metodēm. Parādīts, ka ierobežotas ģeometrijas apstākļos notiek MnO magnētiskā momenta samazināšanās (3.84(4) μ_V/jon. salīdzinot ar 4.892 μ_V/jon. tilpuma materiālam), bet magnētiskās sakārtotības apgabals kļūst būtiski mazāks par nanodaļiņas kodola izmēriem, t.i., uz nanodaļiņas virsmas magnētiskais sakārtojums tiek izjaukts, pie kam MnO nanodaļiņām novērota pāreja no pirmā veida fāžu pārejas uz otro. Tāds pats efekts vērojams mazajās porās esošajam segnetoelektriķim $NaNO_2$. Noteikti nanodaļiņu raksturīgie izmēri un uzņemta sakarība starp fāžu pārejas temperatūru un nanodaļiņu izmēriem. Parādīts, ka daļai nanokompozītu materiālu, kas satur segnetoelektriķus, vērojams straujš efektīvās dielektriskās caurlaidības ε pieaugums augsttemperatūras fāzē, pie kam pie zemām elektriskā lauka frekvencēm ε vērtības sasniedz 10^9.

Алексей Филимонов, Андрей Рудской, Александр Набережнов, Сергей Вахрушев, Екатерина Королева, Игорь Головский, Юрий Кумжеров. Новые нанокомпозитные материалы на основе пористой диэлекрической матрицыВ работе рассматривается влияние условий искусственно ограниченной геометрии на макроскопические свойства, кристаллическую структуру и фазовые переходы в нанокомпозитных материалах на основе пористых матриц с нанометровыми каналами, содержащих внедренные сегнетоэлектрические и магнитные материалы. В качестве пористых матриц использовались пористые стекла со средним диаметром пор 320±20, 46±5, 20±3, 7±1 и 3±0.5 нм, искусственные опалы, хризотиловые асбесты, матрицы SBA-15 с несколькими средними

диаметрами пор в диапазоне 47–87 Å и MCM-41 с порами 24 Å, 35 Å, 47 Å, 68 Å и 87 Å. Магнитные материалы MnO, CoO и Fe_2O_3 непосредственно синтезировались в порах матриц, а сегнетоэлектрики вводились в поры либо из расплава ($NaNO_2$, KNO_3), либо из водного раствора (KH_2PO_4 (KDP), KD_2PO_4 (DKDP), сегнетова соль). Степень дейтерирования DKDP достигала 98 %. Исследования проводились методами дифракции нейтронов и рентгеновского излучения, малоуглового рассеяния нейтронов, электронного парамагнитного резонанса и диэлектрической спектроскопии. Показано, что для MnO в условиях ограниченной геометрии происходит уменьшение магнитного момента (3.84(4) μ_B/ион по сравнению с величиной 4.892 μ_B/ион для массивного материала), а размер области с магнитным упорядочением становится существенно меньше ядерного размера наночастицы, т.е. на поверхности наночастицы магнитный порядок оказывается разрушенным. При этом для наночастиц MnO наблюдается изменение рода фазового перехода от первого рода ко второму. Такой же эффект наблюдается и для сегнетоэлектрика $NaNO_2$ в малых порах. Определены характерные размеры наночастиц и построены зависимости температур фазовых переходов от их размеров. Показано, что для ряда нанокомпозитных материалов, содержащих сегнетоэлектрики, наблюдается резкий рост эффективной диэлектрической проницаемости ε в высокотемпературной фазе, при этом ε достигает значений до 10^9 на низких частотах.